Effects of surface nanostructure and wettability on pool boiling: A molecular dynamics study

International Journal of Thermal Sciences 167 (2021) 106980

Contents lists available at ScienceDirect

International Journal of Thermal Sciences

journal homepage: www.elsevier.com/locate/ijts

Effects of surface nanostructure and wettability on pool boiling: A molecular dynamics study

Armin Shahmardi [a,*], Outi Tammisola [a], Mauro Chinappi [b], Luca Brandt [a]

[a] FLOW and SeRC (Swedish e-Science Research Centre), Department of Engineering Mechanics, Royal Institute of Technology (KTH), SE 100 44, Stockholm, Sweden
[b] Dipartimento Ingegneria Industriale, Università degli studi di Roma Tor Vergata, via del Politecnico 1, 00133, Roma, Italy

ARTICLE INFO

Keywords:
Pool boiling
Bubble nucleation
Molecular dynamics
Wetting
Energy transfer
Nano-structured surfaces

ABSTRACT

We study the role of surface topology, surface chemistry, and wall superheat temperature on the onset of boiling, bubble nucleation and growth, and the possible formation of an insulating vapour film by means of a novel setup for large-scale MD simulations. To minimise the effects of the system size on the bubble growth and the formation of the vapour film, we perform simulations in a box larger than those previously considered. The effect of the system pressure on bubble nucleation and growth is isolated by imposing a constant force on a moving piston and mechanically controlling the pressure. The simulations reveal that the presence of a nanostructure determines the nucleation site and facilitates the energy transfer from the hot substrate to the water. The surface chemistry, on the other hand, governs the shape of the formed bubble. A hydrophilic surface accelerates the bubble nucleation, however, decelerates the bubble expansion, thus postponing the formation of the film of vapour. Hence, a hydrophilic surface provides better energy transfer from the hot wall to the water. By analysing the system energy, we show that irrespective of wall topology and chemistry, there is a wall temperature for which the amount of transferred energy from the wall is maximum.

1. Introduction

Bubble nucleation and pool boiling heat transfer proved to be of great importance in many industries demanding fast and efficient heat transfer from a hot surface (solar energy, thermal power, microfluidic devices, microelectronics and nanoelectronics, to name a few [1,2]). Therefore, during the last decades, several experiments and numerical simulations based on continuum formulations were performed to understand the physics behind bubble nucleation, evaporation/condensation and boiling [3–8].

Among others, Li et al. [9] performed experiments to study the effects of nanostructure surface treatments on boiling performance at low superheat temperatures. They observed enhanced boiling performance due to the formation of nanobubbles induced by stable nucleation sites at microscale cavities. Zupančič et al. [10] studied nucleate boiling on stainless steel foils by visualising nucleating bubbles and temperature fields using high-speed video recording. They showed that bubble nucleation on a flat surface requires higher activation temperature than on a nano-structured surface. Shen et al. [8] employed a diffuse interface model to study bubble growth on a biphilic surface and noticed that, at low gravity, the contact line propagation closely follows the bubble growth everywhere but at the borders between hydrophilic and hydrophobic sections. However, at high gravity, the bubble expansion becomes weaker and the contact line becomes almost stationary at the borders of hydrophilic and hydrophobic sections.

More recently, molecular dynamics (MD) simulations have emerged as a powerful tool to gain detailed information about the physics at the nanoscale also for the case of pool boiling heat transfer. Among the available MD studies, Mao and Zhang [11] studied rapid boiling of a film of water on a hot surface. These authors observed a rapid phase transition of water molecules close to the surface due to the overheating and reported the formation of a constant density non-vaporisation molecular layer attached to the surface of the plate. The effect of the thickness of the liquid film on the phase transition mechanism (evaporation or explosive boiling) was examined by Rabbi et al. [12] by means of MD simulations of liquid argon over a hot wall. According to these results, phase change occurs by evaporation for the two thinner films, whereas the two thicker films undergo explosive boiling. Wang et al. [13] confirmed that the initial thickness of the liquid film strongly affects the onset of explosive boiling. According to their results, the thicker the liquid film, the lower the temperature of onset of boiling. The same authors suggested in another study [14] the existence of a critical film

* Corresponding author.
E-mail address: arminsh@mech.kth.se (A. Shahmardi).

https://doi.org/10.1016/j.ijthermalsci.2021.106980
Received 23 September 2020; Received in revised form 19 February 2021; Accepted 23 March 2021
Available online 6 May 2021

thickness below which the classical nucleation theory fails, when a hydrophilic surface is more suitable for explosive boiling. Gupta et al. [15] studied the onset of bubble nucleation on a partially heated surface by MD simulations and experiments. The effects of the width and the temperature of the heated part of the surface on the bubble growth were explored and a critical radius of nucleation reported.

In order to increase the efficiency of the heat transfer, numerous studies were conducted to design the optimal surface properties when changing the surface chemistry. Hens et al. [16] investigated bubble nucleation and film boiling for different superheat temperatures on surfaces with different chemistry (wettability conditions). These authors reported that hydrophilic surfaces facilitate bubble nucleation or film formation. Zhou et al. [17] studied bubble nucleation over a biphilic surface and observed that the nucleation site moves from the hydrophobic to the hydrophilic part as the superheat temperature increases. Rapid boiling on surfaces with uniform and patterned wettability was investigated by Wu et al. [18]. Their results show that by increasing the hydrophilic degree of the surface, the water temperature increases and the evaporation rate decreases.

As an alternative strategy, changing the topology of the surface can also affect the heat transfer. Fu et al. [19] employed cone-shape nano-structured surfaces to investigate the effects of the size of these patterns on the rapid boiling of a thin water film by means of MD simulations. These authors showed that the nanostructures not only increase the heat transfer from the solid substrate but also affect the temperature history and density distribution. Mukherjee et al. [20] also performed MD simulations to study bubble nucleation of liquid water over a silicon solid substrate, focusing on the effect of the nanostructure height, width and type on the bubble growth rate. Zhang et al. [21] compared the incipient nucleation time and the temperature corresponding to the onset of boiling of liquid argon over three different nano-structured surfaces, namely flat, concave, and convex. Their MD simulations indicate that nano-structured surfaces intensify the bubble nucleation. Moreover the same authors reported that bubble nucleation occurs sooner on a concave nano-structured surface. Zhang et al. [22] show by means of MD simulations that the presence of nanochannels improves the heat transfer from the solid substrate to the liquid argon and intensifies explosive boiling.

Finally, several studies also considered the combined effects of surface chemistry and topology aiming to better control the onset of boiling, bubble nucleation site, boiling heat flux, and the formation of the insulating film of vapour. In particular, phase change of an argon liquid over a nano-structured biphilic substrate was studied by Chen et al. [23] whereas Diaz and Guo [24] conducted boiling simulation of liquid argon placed on a horizontal substrate attached to vertical pillars. Measuring the critical heat flux when varying the pillar arrangement (particularly distance) and surface wettability it was concluded that the critical heat flux increases when increasing the distance between the pillars or increasing the degree of hydrophilic chemistry of the surface (i.e. decreasing the contact angle). Chen et al. [25] studied the bubble nucleation on grooved substrates with different wettability conditions. They reported that the presence of a nanostructure facilitates the boiling heat transfer by both improving the thermal energy transfer and providing an initial bubble nucleus.

It is well known that the bubble nucleation, the temperature of boiling onset, and boiling heat transfer are affected by the pressure of the system as well as by the superheat temperature. While the dependence on different superheat temperatures and surface properties has been studied extensively also at the nanoscale, most of the previous studies do not consider a mechanism to control the pressure. In particular, all the cited works employ MD simulations with fixed volume. This means that the change of the fluid temperature induced by the heat transfer results in a change of the pressure. On the other hand, Marchio et al. [26] showed that standard approaches to perform MD simulations at constant pressure (the so-called NPT runs) provide results which depend on the size of the system when applied to vapour nucleation. It is therefore important to employ a new strategy to control the pressure in MD simulations of boiling systems. As also shown here, see appendix B, the results of the simulations with and without controlling the pressure differ significantly (at least quantitatively).

The goal of this paper is to study bubble nucleation, the formation of the vapour film, and the energy transfer in a pool boiling simulation under controlled pressure when varying the superheat temperature, surface topology and surface chemistry. To properly control the pressure of the system, we choose to mechanically control the pressure by placing a piston above the slab of water as introduced in Ref. [26]. Furthermore, due to the periodicity of the system, the forming bubble usually grows and merges with its periodic image and generates a vapour film at the wall. In order to minimise the effect of the system size on the results, our system is chosen as large as possible given the current computational constraints and the need to explore different superheat and wetting conditions; it consists of more than one million atoms with a substrate area of about 641 nm^2. We will present MD simulations of boiling water for different superheat temperatures and over four different solid substrates: two different kinds of surface chemistry (corresponding to a hydrophilic and a hydrophobic wall) and two different topologies of the solid substrate (a flat wall and a wall with a nano-cavity).

2. System setup and simulation method

The simulated system consists of three main parts: a solid substrate, a water slab, and a solid piston, see Fig. 1. We consider both flat and nano-structured substrates. In both cases, the substrate consists of atoms arranged in an FCC lattice with a lattice parameter equal to 0.33 nm. Fig. 1 displays the computational setup for the case of the nano-structured substrate, where a single cavity is present. The solid substrate has dimensions of 25.33 nm × 25.33 nm × 4.33 nm and is composed of three layers: a bottom fixed layer (black), a thermostated layer (grey) and a free layer (purple). In the case of the nano-structured wall, the width and height of the cavity is 0.08 times those of the solid wall. The interactions among the solid atoms are described by the Lennard-Jones (LJ) potential:

$$V_{ss} = 4\varepsilon_{ss}\left[\left(\frac{\sigma_{ss}}{r}\right)^{12} - \left(\frac{\sigma_{ss}}{r}\right)^{6}\right], \quad (1)$$

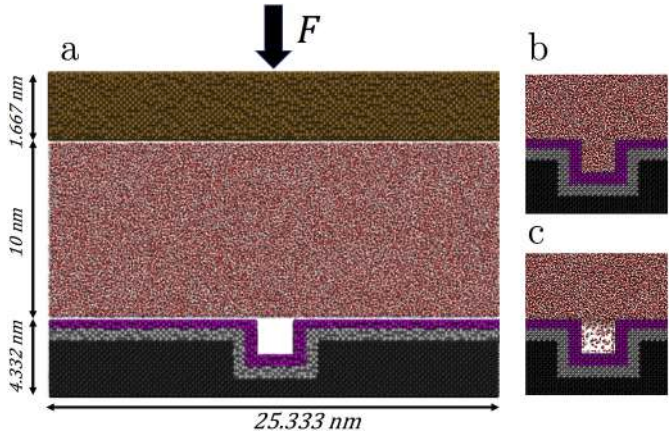

Fig. 1. Simulation set-up. a) The simulation system is composed of three components: a solid substrate, a water slab, and a solid piston. The solid substrate consists of three layers, namely the frozen layer (black), the thermostat layer (grey), and the free layer (purple). The components and the layering are the same for the flat substrate for which the cavity is also filled with solid atoms. For nano-structured walls, the stationary state reached at the end of the equilibration phase can be either the Wenzel or Cassie-Baxter state. For a hydrophilic cavity, we obtain Wenzel state (cavity completely filled by the liquid, panel b) whereas for a hydrophobic cavity, the Cassie-Baxter state (liquid does not fill the cavity, panel c). (For interpretation of the references to colour in this figure legend, the reader is referred to the Web version of this article.)

where $\sigma_{ss} = 0.216$ nm is the distance at which the intermolecular potential between the two atoms is zero and $\varepsilon_{ss} = 40$ kJ/mol is the depth of the potential well. The LJ parameters are selected such that the maximum temperature of the simulations (700 K) is below the melting temperature of the solid substrate. All the LJ interactions are cut beyond a distance $r_c = 0.9$ nm. The positions of the first layer of the substrate (black in the figure) atoms are frozen. During the non-equilibrium simulations, atoms in the thermostated (purple) region are restrained to their initial lattice positions through a harmonic potential:

$$V_{pr}(\boldsymbol{r}_i) = \frac{1}{2} k_{pr} (\boldsymbol{r}_i - \boldsymbol{R}_i)^2, \tag{2}$$

where $\boldsymbol{r}_i$ is the position of atom i at time t, $\boldsymbol{R}_i$ is the initial position of atom i, and $k_{pr} = 10^3$ kJ/(molnm^2) is the spring constant. Moreover, atoms in the thermostated region are connected to a velocity rescale thermostat [27].

To properly control the pressure, a piston (brown atoms in Fig. 1) is placed on top of the water slab. This is free to move up and down thus providing a mechanical control of the pressure as introduced in Ref. [26]. The piston is also modelled as an FCC solid with same lattice parameter as the substrate. The height of the piston is 3.66 nm. A constant downward acceleration is imposed on all the atoms of the piston, with magnitude computed to provide the force on the piston which corresponds to the prescribed pressure. In particular, being F the total downward force acting on the piston, f the downward force on each atom, A the area of the piston and n_p the number of atoms of the piston, we have:

$$P = \frac{F}{A} = \frac{f n_p}{A}. \tag{3}$$

Although the proposed pressure control algorithm proved to be reliable in atomistic simulations of vapour nucleation (see Ref. [26]), we examined it by performing a test where we measure the displacement of a solid wall connected to a spring when subjected to a constant downward pressure force (see appendix A).

Finally, the SPC/E model [28] is used for water. The height of the water slab is $\simeq 10$ nm, with periodicity assumed in all the three directions. It is worth to mention that the simulation box is considered high enough (200 nm) to avoid any short range interaction between the piston at the top and the periodic image of the solid substrate as well as any significant long range interaction.

For the single cavity reported in Fig. 1, the system contains around 1.2 million atoms including (approximately) 190k atoms in the frozen layer, 54k atoms connected to the thermostat, 62k atoms in the free layer of the solid wall, 630k atoms in water slab (to be precise 209876 water molecules), and 250k atoms forming the piston.

2.1. Wettability of the substrate

The wettability of the substrate is controlled by the water-substrate interaction potential. The oxygen atoms of water molecules interact with the solid atoms via a Lennard-Jones potential

$$V_{so} = 4\varepsilon_{so}\left[\left(\frac{\sigma_{so}}{r}\right)^{12} - \left(\frac{\sigma_{so}}{r}\right)^{6}\right], \tag{4}$$

where σ_{so} is equal to the arithmetic average of $\sigma_{ss} = 0.216$ nm and $\sigma_{oo} = 0.317$ nm, according to the Lorentz-Berthelot rule [29]. The value of ε_{so} controls the wettability. Several wetting simulations were performed on a cylindrical droplet [30] for different values of ε_{so} to obtain the values corresponding to a hydrophobic and a hydrophilic surface. In particular, we have selected $\varepsilon_{so} = 0.55$ kJ/mol for an hydrophobic substrate (contact angle $\theta \approx 135^\circ$) and $\varepsilon_{so} = 1.4$ kJ/mol for the hydrophilic substrate (contact angle $\theta \approx 45^\circ$). Fig. 2 presents the equilibrium configuration from the wetting simulations over the hydrophilic and hydrophobic flat walls. Note that the contact angles are measured graphically and the reported angles are approximated values which are accurate enough for our purpose (i.e. providing a hydrophilic and a hydrophobic surface).

2.2. Simulation protocol

All the simulations are performed using the open-source software GROMACS [31]. The simulation protocol is as follows. First, each of the three components of the system (solid substrate, water slab, and piston) are separately equilibrated for 1 ns. The solid substrate is equilibrated at $T = 300$ K using an NVT simulation. To this aim, all the three layers are connected to a velocity rescaling thermostat for 1 ns. The piston is also equilibrated at $T = 300$ K using the same thermostat. Finally, the water slab is equilibrated using an NPT semi-isotropic simulation where a Parrinello-Rahman barostat [32] is used together with a velocity rescaling thermostat to equilibrate the water box at $T = 300$ K and $P = 1$ bar.

Secondly, the equilibrated components are combined as shown in Fig. 1. An additional NVT equilibration is then performed on the integrated system for 1 ns. During this run, the piston is active, i.e. a constant acceleration (or equivalently a constant force) is applied on each atom forming the piston. Depending on the magnitude of the mechanically applied pressure and on the chemistry of the surface, the stationary state reached by the system after this equilibration phase can be either a Cassie-Baxter or a Wenzel state [33–36]. The system spontaneously moves to a Wenzel state (the cavity is completely filled by the liquid) for the hydrophilic cavity, whereas the stationary state for a hydrophobic nano-structured wall is a Cassie-Baxter state (the liquid does not fill the cavity). Finally, the thermostat is disconnected from all the atoms except those in thermostat group of the solid substrate (see Fig. 1) and the non-equilibrium molecular dynamics simulations are started.

As introduced above, we shall study two substrates, namely, a flat wall and a nano-structured wall. For each substrate, two different wettabilities are studied, hydrophobic and hydrophilic (indicated as $\theta > 90^\circ$ and $\theta < 90^\circ$ in the figures). Seven thermostat temperatures are considered, $T_W = 400$ K, 450 K, 500 K, 550 K, 600 K, 650 K, and 700 K. For all the simulations we use a time step of 0.1 fs except for those at temperature larger than 550 K when the time step is reduced to 0.05 fs. For the sake of computational cost, the simulations are limited by two criteria. i) Simulations are performed up to maximum 8 ns, or ii) they are stopped when the vapour film completely covers the wall, because we are only

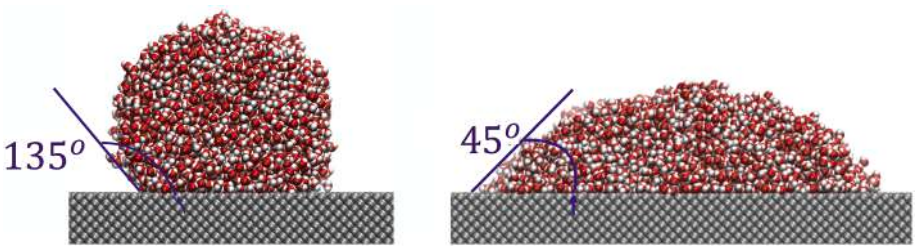

Fig. 2. Wettability simulations. Droplet equilibrium over a hydrophobic and hydrophilic wall. The results show that the contact angles for the hyrdophobic and hydrophilic walls are about 135° and 45°.

interested in the physics prior to the formation of the vapour film, i.e. when the solid substrate is not fully insulated by the vapour film.

3. Results

The results of the simulations of boiling on surfaces with different topologies and wettabilities will be analysed in terms of bubble formation, location of the nucleation site, bubble growth, film formation, and energy transfer from the hot wall to the water slab and the piston.

3.1. Bubble nucleation and bubble growth

The formation, the shape, and the growth of the bubble or the formation of the vapour film strongly depend on the topology and the chemical properties of the wall. Fig. 3 displays the evolution of the nucleated bubble for the case with the thermostat temperature of 700 K (hereafter this will be referred to as wall temperature and denoted by T_W) for the 4 different wall chemistries and topologies under consideration.

We detect the bubble nucleation and the onset of boiling by calculating the average density fields. To this end, the simulation domain is divided into a finite number of numerical cells ($1nm \times 1nm \times 25.33nm$) and the position of each water molecule defined by the position of the oxygen atom. We count the number of molecules in each numerical cell and average first in the groove direction (perpendicular to the plane in Fig. 1). The averaged density as a function of time is then computed with the averaged number of water molecules in each cell, the molecular mass of a water molecule, and the volume of each numerical cell. The instant when the density decreases below a selected threshold, and remain below it, is taken as the nucleation time. The threshold value is selected close to the water vapour density at $1bar$ and corresponding temperature.

For the nucleation to happen, water molecules should absorb enough thermal energy to overcome an energy barrier. According to Fig. 3, the presence of a nano-cavity provides a preferable nucleation site. For a hydrophilic nanostructured wall, when the initial state after equilibration is the Wenzel state [34] (i.e. the water completely occupies the cavity as shown in Fig. $3a_1$), the water molecules inside the cavity are adjacent to a larger solid surface area and interact with more atoms of the solid wall. Therefore, more thermal energy is absorbed by the water molecules inside the cavity than by those adjacent to the flat part of the wall; hence, the bubble always nucleates inside the cavity (see Fig. $3a_2$). On the contrary, for a hydrophobic structured wall, the initial state is the Cassie–Baxter state [33] (see Fig. $3b_1$) i.e. an initial residual gas phase is trapped inside the cavity. As a result, the nucleation occurs around the nanostructure as illustrated in Fig. $3b_2$, see also the results in Ref. [25].

Bubble nucleation occurs in random locations over the flat walls. For the hydrophilic case, the nucleation is observed randomly in the bulk liquid (Fig. $3c_2$), as documented in Fig. 4 where we depict the nucleation site over a flat hydrophilic wall from simulations with wall temperature $T_W = 600$ K and $T_W = 650$ K.

Similarly, bubble nucleation appears at random locations but at the wall for the case of a hydrophobic flat wall. We magnify frames $3d_2 - d_5$ in Fig. 5 to elaborate on the mechanism behind the formation of an insulating film in this case. As shown in panel a of the figure, there is no unique nucleation site (see the black dashed circles), and the boiling starts with several nucleation sites. The bubbles soon merge and form larger bubbles, see Fig. 5b. The large bubbles, in turn, grow (Fig. 5c) and merge to form the insulating film of vapour (Fig. 5d).

As concerns the nucleation time, our results suggest that regardless of the surface topology, bubble nucleates sooner on the hydrophilic walls. As shown in Fig. $3a_2$ and Fig. $3b_2$, the nucleation occurs at $t \simeq 1.325$ ns over a hydrophilic nano-structured wall whereas it is observed at $t \simeq 4.85$ ns over a hydrophobic nano-structured wall. This observation suggests that a hydrophilic surface facilitates the heat transfer, as discussed later in section 3.2 by analysing the mechanisms for energy transfer at work. Depending on the surface chemistry, the presence of a cavity either accelerates or decelerates the bubble nucleation. For a hydrophilic nano-structured wall, the water molecules inside the cavity absorb more thermal energy so that the bubble nucleation is accelerated (compare Fig. $3a_2$ and Fig. $3c_2$). Conversely, the water molecules around the hydrophobic cavity interact with fewer atoms of the hot solid as the preferable nucleation site is filled with gas. Therefore, a hydrophobic nanostructure postpones the bubble nucleation (compare Fig. $3b_2$ and Fig. $3d_2$). Note that the effects of the surface topology on the nucleation time are more evident for the hydrophilic walls.

The nucleated bubble requires additional thermal energy to grow and form the insulating vapour film [25]. Since for a nano-structured wall the initial bubble forms in the cavity (see Fig. $3a_2$ and Fig. $3b_2$), some parts of the solid wall inside or around the nanostructure are insulated. Hence, the interactions (or energy transfer) between the atoms of the hot solid wall and the water molecules surrounding the bubble decrease. As the bubble grows in size, the portion of the wall which is insulated by the film of gas increases (see Fig. $3a_3 - a_5$ and Fig. $3b_3 - b_4$). Note, however, that, in the case of a flat hydrophilic wall, the nucleus is forming in the bulk liquid, surrounded by water molecules. Therefore, there is no insulation of the solid wall and the water molecules around the nucleus absorb more thermal energy than in the case of a bubble around the cavity. In addition, for a hydrophobic flat wall, see Fig. $3b_2$ and Fig. $3d_2$, a greater portion of the solid wall is insulated in the presence of the cavity. Hence, the bubble grows slower on a nano-structured wall and the insulating film forms later than over a flat wall.

Note that, as also discussed above, although the rate of the absorbed energy from a flat wall after nucleation is greater than that absorbed from the nano-structured wall, the time needed for the film to form is shorter. In particular, it takes about 0.625 ns for the nucleated bubble over a hydrophilic nano-structured wall (see Fig. $3a_2$) to grow and form the film (see Fig. $3a_7$) whereas the same process takes 0.15 ns on a hydrophilic flat wall (see Fig. $3c_2$ and Fig. $3c_5$). Therefore, the total amount of the energy transferred after the nucleation is greater for a nano-structured wall due to the delay in the film formation.

Finally, comparing Fig. $3a_2 - a_5$ and Fig. $3b_2 - b_4$, we see that the surface chemistry dictates the shape of the nucleated bubble. Over a hydrophilic wall, the contact angle is always acute ($\theta < 90$) while the bubble is growing, whereas it is always obtuse ($\theta > 90$) for a hydrophobic wall (compare Fig. $3a_4$ and Fig. $3b_3$).

3.2. Energy analysis

In the following, we will consider the system consisting of the water slab and the piston and examine the total amount and the rate of energy transfer from the bottom wall to the system, denoted as ΔE and $\dot{E}$. The total energy of the system is computed as the sum of five different contributions:

$$E = U_w + K_w + U_p + K_p + U_s \tag{5}$$

where U_w (water potential energy) is the summation of the Lennard-Jones and the Coulomb interaction energy among the water molecules, K_w is the kinetic energy of the water atoms, U_p is the Lennard-Jones interaction energy among the piston atoms, K_p represents the kinetic energy of the piston atoms, and finally, U_s is the sum of all the surface energies, i.e. the Lennard-Jones interaction of the water atoms with the wall and the piston atoms.

There are two mechanisms contributing to the energy transfer to the system. The first and dominant one is the short range molecular interactions which strongly depend on the surface wettability; for a hydrophilic surface, the interactions between the molecules of the hot solid wall and the liquid film are much stronger than those of a hydrophobic wall. The second mechanism is the translational motion of the molecules within the liquid film. This mechanism requires high temperature gra-

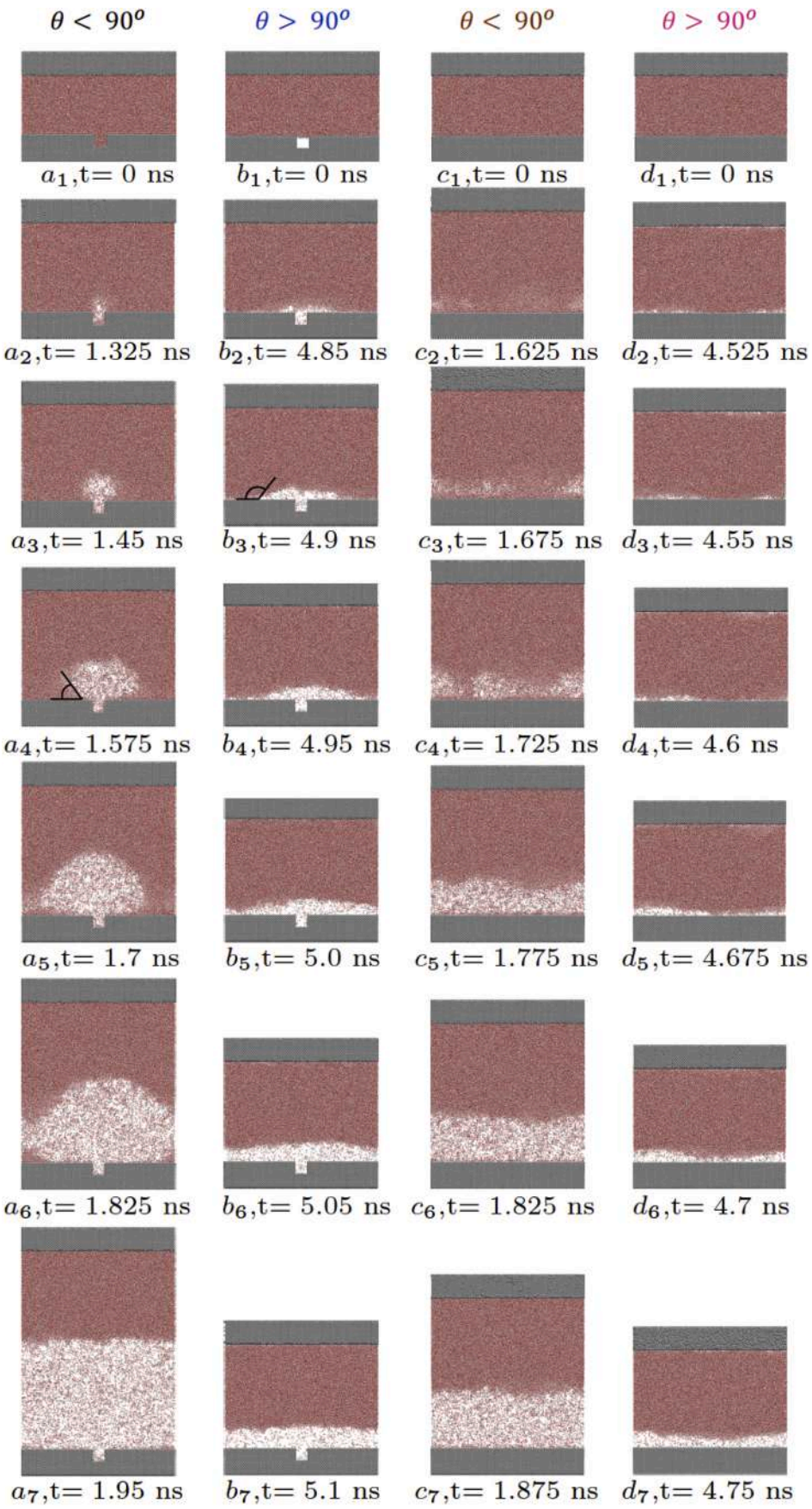

Fig. 3. Evolution of the nucleated bubble for different wall chemistries and topologies. The thermostat temperature is set to $T_W = 700$ K. The first and the second columns correspond to nanostructured walls while the third and the fourth columns show the evolution of the bubble (or the film) on a flat wall. The walls in the first and the third columns are hydrophilic whereas the walls in the second and the fourth columns are hydrophobic. The presence of a nanostructure mostly controls the nucleation site, whereas the bubble shape depends on the surface chemistry.

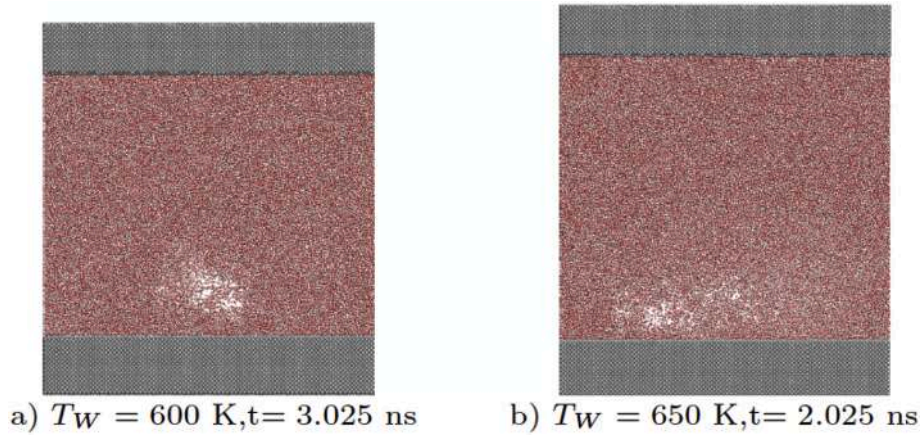

Fig. 4. Random nucleation over a heated hydrophilic flat wall. The two panels report the first stage of the nucleation for (a) T_W = 600K, b) T_W = 650K.

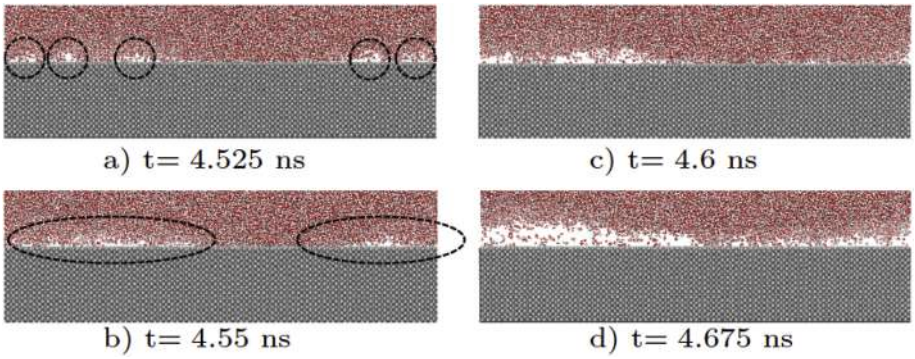

Fig. 5. Bubble nucleation over a hydrophobic flat wall. In this case, there is no unique nucleation site. Bubble nuclei form in several random locations at the wall and merge quickly to form a vapour film.

dients within the film. Wang et al. [14] referred to these two mechanisms as molecular collisions and heat convection, and showed that their relative importance depends on the initial thickness of the liquid film. According to the results in Ref. [14], given a surface chemistry, there is a critical thickness of the liquid film below which the temperature is relatively uniform within the film; hence, the translational motion of the molecules is negligible and the classical nucleation theory fails, i.e. a hydrophilic surface yields a favourable heat transfer. We will therefore discuss our results in the light of these findings, recalling that the initial thickness of the water slab in our simulations (after the equilibration) is ≈ 9.7 nm.

To analyse the energy transfer in the system, we first investigate the translational molecular motion. To this end, we borrow the idea of Wang et al. [14] and examine the distribution of the averaged temperature

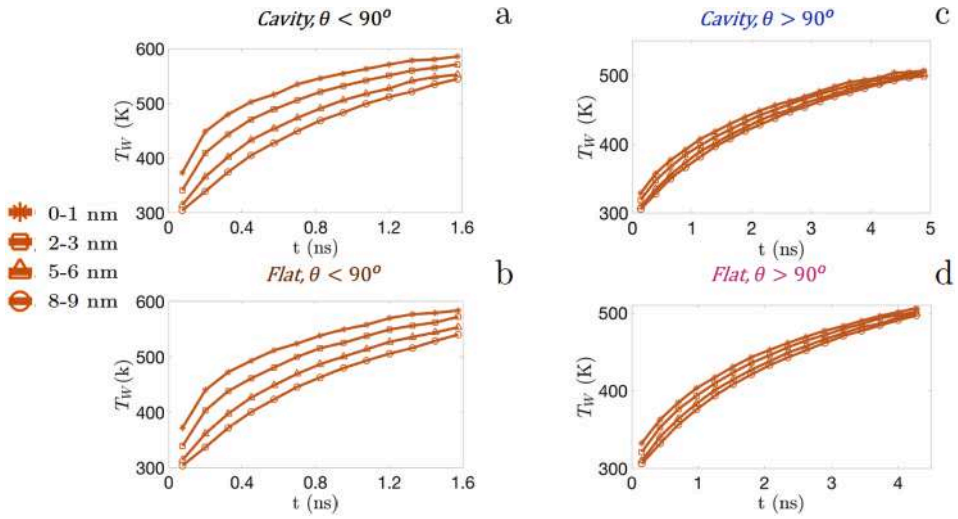

Fig. 6. Evolution of the averaged water temperature in four different layers above the solid wall. For the hydrophobic walls, the negligible difference between the temperature of the first and the fourth layer indicates that the translational motion of the molecules is negligible and the molecular interaction is the main heat transfer mechanism.

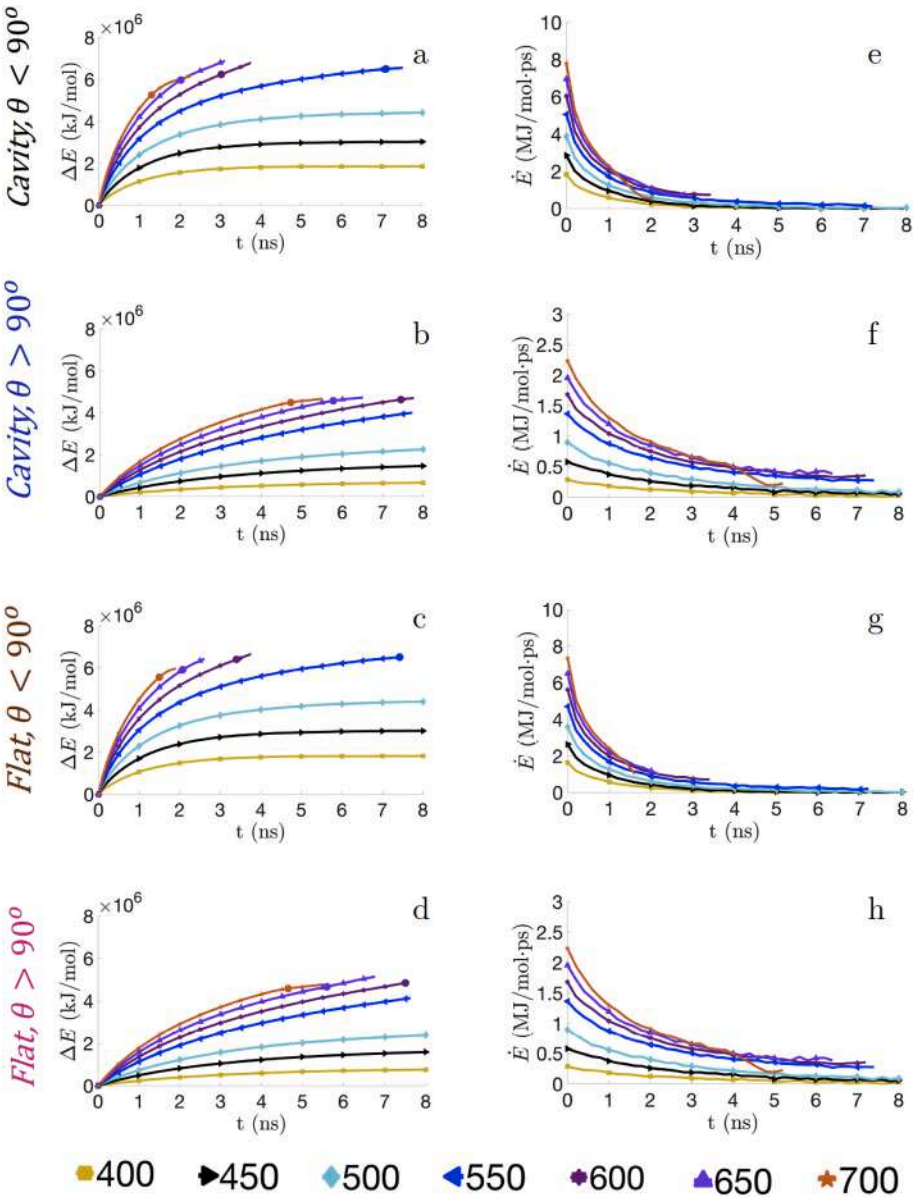

Fig. 7. Time evolution of the system energy and of its rate of change. Panels a–d depict $\Delta E = E(t) - E_0$ with E_0 the initial energy while panel e–g the rate of change $\dot{E} = dE/dt$ for the four combination of wall wettability and topologies under consideration. The onset of boiling, when observed, is indicated with a filled circle in the energy plot, see e.g. the red circle in panel a), which corresponds to the visualisation in panel a) of Fig. 3. For some cases, boiling does not start during the 8*ns* of the simulation. (For interpretation of the references to colour in this figure legend, the reader is referred to the Web version of this article.)

along the water slab thickness for the case with wall temperature of 700K (see Fig. 6). We consider four layers of water, corresponding to $\Delta z = 0-1$ nm, $\Delta z = 2-3$ nm, $\Delta z = 5-6$ nm, $\Delta z = 8-9$ nm, where $\Delta z = z - z_{sub}$, and $z_{sub} = 4.332$ nm is the height of the substrate.

The data in Fig. 6a and b, reveal that the difference between the temperature of the first and the last layer ($0-1nm$ and $8-9nm$) is greater for the hydrophilic walls than for the hydrophobic walls. Therefore, besides the molecular interactions, heat transfer is also due to the translation of the water molecules in the case of the hydrophilic walls. On the other hand, the difference between the temperature of the first and the last layer is negligible for the hydrophobic walls (see 6c and 6d). Hence, the main mechanism for heat transfer is the molecular interaction. Therefore, considering stronger molecular interactions between the hydrophilic solid wall (comparing to the hydrophobic solid wall) and the water molecules, the hydrophilic surface provides better heat transfer.

In Fig. 7, we report the time evolution of the system total energy, $\Delta E = E(t) - E_0$ (where E_0 stands for the initial energy of the system), and its rate of change, $\dot{E} = dE/dt$, for the different wall surface chemistry and topologies under consideration. To reduce the noise, $\dot{E}$ is obtained as an average over time intervals of 200 ps.

Some general conclusions can be drawn from the data in Fig. 7. First, both the energy of the system, E, and its rate of change, $\dot{E}$, are more affected by the change in the chemistry of the surface rather than by the topology of the wall.

For a hydrophilic wall, the water molecules absorb a large amount of energy from the hot wall through strong molecular interactions (see Fig. 7a–c). Then, due to the large temperature gradient between the different layers (see Fig. 6a and b), the absorbed energy is transferred to the upper layers of water atoms through both molecular interactions and the migration of hot water molecules to the colder part of the system. Due to this energy transport within the system, the layer of water atoms close to the wall can absorb more energy before breaking the energy barrier of nucleation. Note that the presence of the piston (or controlled pressure of the system) prevents evaporation to occur before the system absorbs enough energy to overcome the energy barrier. According to Fig. 6a and b, the difference between the temperature of the different layers of the water slab decreases over the time resulting in a reduction of the translational molecular motion. Thus, approaching the nucleation time, most of the energy absorbed from the wall remains close to the wall.

For a hydrophobic wall, on the other hand, the temperature gradient within the water slab is negligible (see Fig. 6c and d); hence, energy is transferred from the hot wall to the system mainly through the molecular interactions. Because of the weaker molecular interactions between the solid wall and water molecules, the increase of the system energy is slower and less intense as seen in Fig. 7. Therefore, the energy required to overcome the energy barrier and nucleate the bubble (or form the vapour film) is provided over a longer time for a hydrophobic wall. This observation is consistent with the results in section 3.1 where it was shown that the bubble (or the film) inception time is mainly affected by the surface chemistry; as an example, in the case of the nano-structured topology, nucleation occurs after 1.325 ns over a hydrophilic wall (Fig. 3a_2) whereas it requires 4.85 ns in the case of a hydrophobic wall (Fig. 3b_2).

Moreover, we see that ΔE and $\dot{E}$ increase with the wall temperature before the onset of boiling for all the cases (the time corresponding to the onset of boiling is marked with symbols in the plots in the first row of Fig. 7). Note, however, that boiling does not start during the $8ns$ of simulations for some of the cases due to low rate of energy transfer in those systems.

Finally, after the onset of boiling, the hot wall is partially insulated by the vapour phase. Therefore, the interactions between the atoms of the hot solid wall and the water molecules decrease dramatically and the total energy of the system approaches a plateau.

Next, we report in Fig. 8 the effect of different wall temperatures, T_W, on the maximum amount of energy extracted from the hot wall by the water slab, ΔE_{max}, and the maximum rate of energy transfer between the hot wall and the system, $\dot{E}_{max}$ (Fig. 8a and b). The maximum amount of transferred energy, ΔE_{max}, first increases with the wall temperature and then decreases. This behaviour is attributed to the combined effects of bubble formation and growth and to the increase of the rate of energy transfer at high temperature.

Consistently with the discussion above, $\dot{E}$ decreases with time, see Fig. 7e–h. This is in agreement with the standard continuum intuition that suggests that $\dot{E}$ is roughly proportional to the temperature difference between the solid wall and the temperature of the portion of the water slab in contact to the wall. This difference is maximum at the beginning of the process when the water slab is at 300 K and it decreases as the water temperature increases over the time. Moreover, the higher the wall temperature, the more the rate of the energy transfer. On the other hand, for the highest wall temperatures, the vapour bubble forms sooner and grows faster. Thus, an insulating vapour layer partially or fully covers the wall relatively quickly, which results in a reduction of the energy transfer. Therefore, for a given wall toplogy and chemistry, the maximum amount of the energy transfer is a trade off between the rate of the energy transfer (which increases with wall temperature) and the formation of the insulating film (which occurs earlier for higher wall temperatures). These two mechanisms explains the presence of a maximum in Fig. 8a.

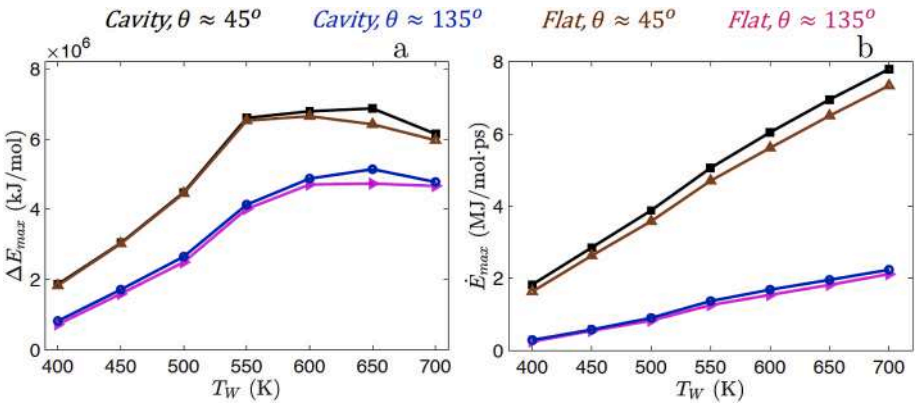

Fig. 8. Effect of wall temperature on the energy transfer. a) Maximum amount of energy extracted by the water slab from the hot wall and b) maximum rate of change of the energy of the system. Although the maximum rate of energy transfer ($\dot{E}_{max}$) increases with the wall temperature, the maximum amount of transferred energy, ΔE_{max}, first increases with the wall temperature and then decreases.

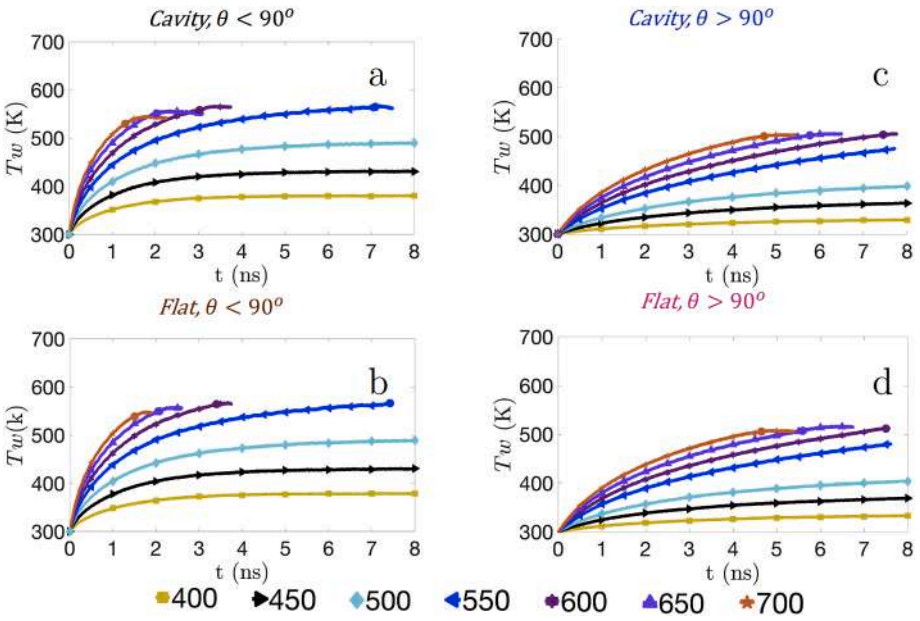

Fig. 9. Evolution of the average water temperature. Due to the formation of the insulating vapour film, the averaged water temperature never reaches the thermostat temperature.

As mentioned earlier, the chemistry of the wall has a dominant role for the amount of energy transfer to the system. However, according to Fig. 8a, given the surface chemistry, the wall temperature at which the amount of transferred energy is maximum differs for the different surface topologies. In particular, the temperature corresponding to the maximum transferred energy is higher for the cases with nano-structured surfaces than for the flat walls. Considering the discussion above about the origin of the maximum in the energy transfer curve in Fig. 8a, the data confirm that the surface topology also affects the bubble growth and the formation of the film (although less than the surface chemistry). For nano-structured surfaces, the bubble forms and grows around the cavity and its growth rate is therefore limited as it was discussed in section 3.1. Thus, a nanostructure delays the formation of the vapour film and improves the energy transfer which is in agreement with the results of the experiments performed by Das et al. [37]. Their results illustrate that nano-structured surfaces increase the pool boiling heat transfer by increasing the effective heating surface.

3.3. Temperature fields

The evolution of the averaged temperature of the water (*Tw*) is displayed in Fig. 9 for the different wall topologies, types of surface

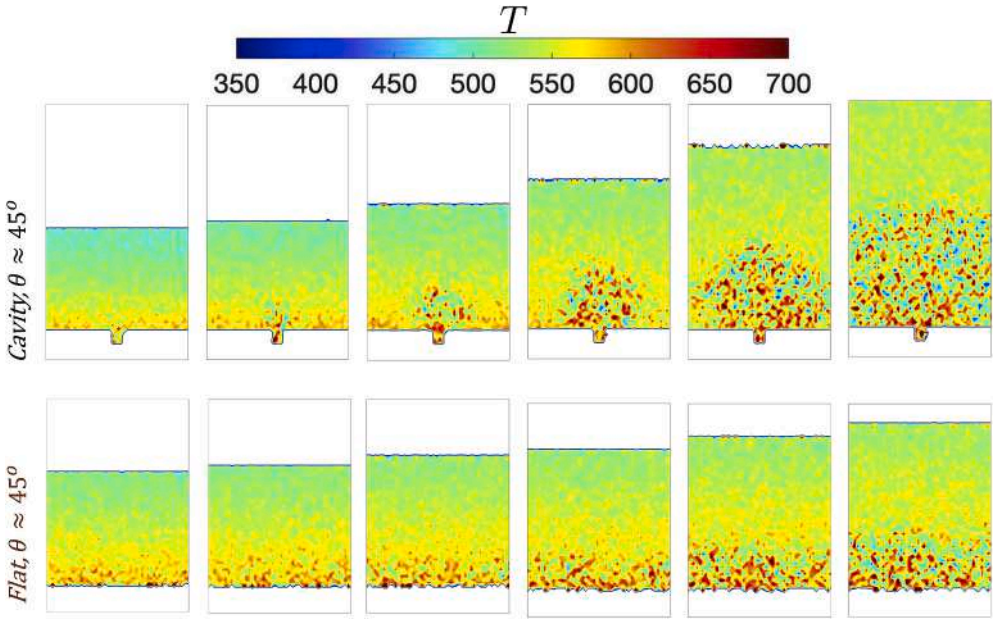

Fig. 10. Time evolution of the instantaneous water temperature field for the hydrophilic cases. $T_W = 700$ K. Although the averaged wall temperature is below that of thermostat, the water temperature reaches the thermostat temperature locally.

chemistry, and different thermostat temperatures examined. Note that the values of temperature in Fig. 9 are the average over the whole water slab; the filled circles represent the averaged temperature of the water at the onset of boiling and should not be considered as the onset of boiling temperature.

First we note that for all cases, irrespective of the wall chemistry and topology, the averaged water temperature does not reach that of the wall during the 8 ns of simulation. Let us consider the hydrophilic structured wall (Fig. 9a) for which the bubble nucleation, bubble growth, and film formation occur during the simulation time if the wall temperature is greater than 500 K. For these wall temperatures, the vapour phase insulates the hot wall partially (or fully) before the averaged water temperature reaches that of the wall. Therefore, the averaged water temperature is always below the wall temperature.

As discussed earlier, higher wall temperatures accelerate the onset of boiling and the formation of the insulating layer. As a consequence, in the case where the wall temperature is 700 K, the difference between the equilibrium water temperature (around 550 K) and the wall temperature is higher than that at the lower temperatures. Note also that for the cases with thermostat temperatures equal and below 500 K, the average water temperature is still slightly increasing with time, which indicates that longer simulation times would be necessary to reach the equilibrium temperature and observing bubble nulceation. Although the averaged water temperature is always below the wall temperature, locally the water temperature does reach that of the wall. This is documented in Fig. 10 by iso-contours of instantaneous local temperature of the water molecules for the boiling over hydrophilic walls and thermostat temperature 700 K, where the time frames are selected at the same instances as those in Fig. 3. Indeed, as suggested by the visualisations in Fig. 3, the local temperature is higher inside the cavity at the onset of the boiling, where it is close to the wall temperature (see Fig. 10 a) and where nucleation is therefore seen. As time evolves, the region of high local temperature expands on the upper surface (cf. Fig. 10b–f), leading to bubble growth and the formation of the film, as also discussed earlier. Similarly, at the onset of boiling over the flat hydrophilic wall, the local temperature is highest at the nucleation site, close to the wall temperature (see above the left part of the wall in Fig. 10 m).

Finally, let us consider Fig. 9a and c (or Fig. 9b and d). The results reveal that for a given surface chemistry and wall temperature, the averaged temperature of the system corresponding to the onset of boiling (filled circles on the plots) is greater if the wall is not nanostructured. This observation is in agreement with the experimental study by Zupančič et al. [10]. Their results show that the bubble nucleation on a flat surface requires higher activation temperature than on a nano-structured surface.

4. Conclusion

The onset of boiling, bubble nucleation and growth, and the possible formation of an insulating vapour film are investigated by means of large-scale MD simulations and analysing the system energy evolution. In particular, we consider a hydrophilic and a hydrophobic wall and two wall topologies, a flat wall and a wall with a periodic array of nanocavities, and vary the temperature of the solid substrate from 400 K to 700 K. Specific and novel to this set of simulations is the control of the system pressure by means of a piston on the top boundary. A downward constant force is imposed on the piston atoms providing a mechanical control of the averaged pressure of the system at the desired value ($P = 1$ bar).

The results of the simulations with different wall topologies reveal that the presence of a nanostructure triggers the bubble formation for a hydrophilic wall and postpones it for a hydrophobic wall. Irrespective of the surface chemistry, the nanostructure also provides a preferable nucleation site due to a larger solid surface in contact with the liquid in the nanostructure (for a hydrophilic wall) and a residual gas phase trapped in the cavity (for a hydrophobic wall). Our results suggests that the presence of a nanostructure delays the formation of the insulating film; the formed bubble expands around the nanostructure, thus partially insulates the wall. As the bubble grows, the portion of the wall insulated by the gas phase increases gradually resulting in a decrease of the energy transfer from the wall. Hence, the insulating vapour film forms over a longer period of time on a nano-structured wall when comparing to the film formation on a flat wall. Therefore, the presence of a nanostructure facilitates the energy transfer from the hot substrate to the water by controlling the nucleation site, detaining the bubble growth, and postponing the formation of the vapour film.

Concerning the wall chemistry, we show that a hydrophilic wall facilitates the energy transfer. This is explained by examining two possible mechanisms for energy transfer within the system; namely, the molecular interactions and the translational motion of the water molecules within the system. For the cases with hydrophilic walls, due to high temperature gradient within the different water layers, the migration of the hot water molecules towards the piston distributes the energy in the system, in addition to molecular interactions. Hence, more energy can be absorbed from the hot wall before nucleation. Moreover, the molecular interactions between the water molecules and the atoms of a hydrophilic solid wall are more intense than those with a hydrophobic wall. In addition, on a hydrophobic wall, the negligible temperature gradient within the water slab prevents any observable molecular migration. Thus, the absorbed energy is mostly accumulated in vicinity of the wall, so that a hydrophilic surface accelerates the bubble nucleation. This surface chemistry however decelerates the bubble expansion, thus postponing the formation of the film of vapour. Therefore, a hydrophilic surface provides a better energy transfer from the hot wall to the water.

Regardless of the surface topology and chemistry, we have shown that the maximum amount of energy transfer between the hot wall and the water increases with the wall temperature at the lowest temperature values considered (from 400 K to approximately 550 K depending on the wall topology). We explain this increase by quantifying the maximum rate of energy transfer, which is also increasing with the wall temperature. Further increasing the wall temperature, the maximum amount of energy transfer undergoes a reduction. This reduction is a consequence of the formation of the vapour film which insulates the wall. Higher wall temperature accelerates bubble nucleation, bubble growth, and the formation of the film of vapour. Therefore, irrespective of the wall topology and chemistry, we find a wall temperature for which the amount of transferred energy is maximum. Finally, our simulations show that although the averaged temperature of the system is always below the wall temperature, the temperature locally reaches that of the thermostat in the nucleation site and this hotter region grows in size as the bubble expands.

In summary, despite the known limitations of the MD approach (e.g. short time scale, small systems, need for large superheat), we show that large-scale simulations provide a viable tool to shed light on the combined effect of chemistry and nanostructure on the first stages of pool boiling. The possibility to accurately control pressure, wall chemistry and nanostructure shape, combined with the increasing computational performance of GPU systems, paves the way to the use of this approach to explore more complex scenarios such as biphilic surfaces and reentrant textures.

Declaration of competing interest

The authors declare that they have no known competing financial interests or personal relationships that could have appeared to influence the work reported in this paper.

Data availability

Data will be made available on request.

Acknowledgement

The research was financially supported by the Swedish Research Council, via the multidisciplinary research environment INTERFACE (VR 2016–06119 "Hybrid multiscale modelling of transport phenomena for energy efficient processes"). The computation resources were supported by a grant from the Centro Svizzero di Calcolo Scientifico (CSCS) under project ID s864.

Appendix A. Validation of pressure control algorithm

Fig. A.11a illustrates the simulation setup for validating the pressure control algorithm. This small system contains three components, namely, a piston (brown), a water slab, and a substrate (grey), similar to the setup of [26]. The idea is to impose a constant force (corresponding to a desirable pressure) on the piston and obtain the prescribed pressure at the substrate. Therefore, all the atoms of the piston are subjected to a constant downward force. The atoms in the substrate are connected to a spring with constant of $k_{pr_A} = 1\ \mathrm{kJ/(molnm^2)}$.

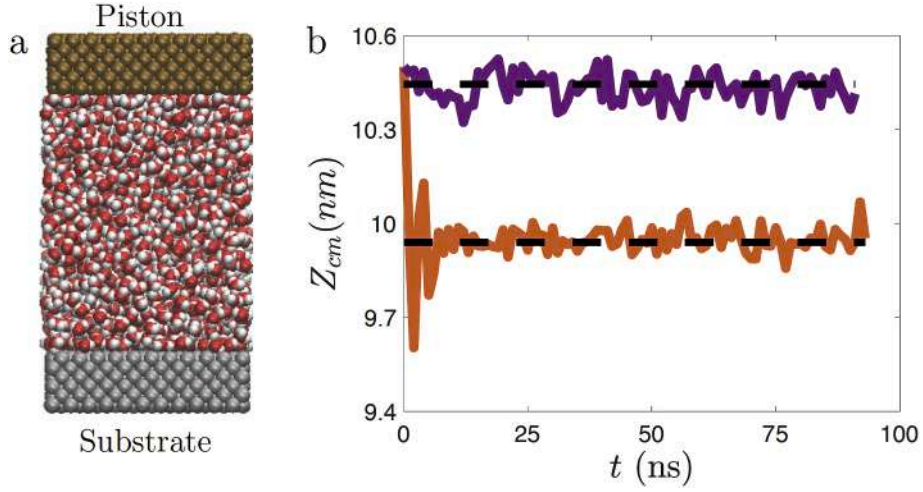

Fig. A.11. a) System setup for examining the pressure control algorithm. The system consists of three parts. A piston (brown atoms) on which a constant force is imposed, water molecules, and the substrate atoms (grey) which are connected to a spring with constant of $k_{pr_A} = 1\ \mathrm{kJ/(molnm^2)}$. b) Evolution of the substrate height when subject to downward forces of two different magnitudes. Purple and orange solid lines represent the results for $f_{p_1} = 9.26 \times 10^{-14}$ N and $f_{p_2} = 9.26 \times 10^{-13}$ N. The black dashed lines show the averaged height of the substrate.

Given the number of atoms in the piston, $n_{p_A} = 1452$, and the area of the piston $A_{p_A} = 3.66$ nm $\times$ 3.66 nm, we can calculate the force $f_{p_1} = 9.26 \times 10^{-14}$ N and $f_{p_2} = 9.26 \times 10^{-13}$ N needed to obtain the desired pressure $P_1 = 100bar$ and $P_2 = 1000bar$ as

$$f = \frac{PA_{p_A}}{n_{p_A}} \tag{A.1}$$

Next, we impose the calculated downward forces on each atom of the piston and perform a NVT simulation at 300K. Fig. A.11b shows the evolution of the substrate height (height of the center of mass of the substrate, z_{cm}) corresponding to an average displacement ($\overline{\Delta Z_{cm}}$) -0.056 nm and -0.56 nm for f_{p_1} and f_{p_2}. We calculate the pressure at the substrate as

$$P = \frac{n_{sub_A} k_{pr_A} \overline{\Delta Z_{cm}}}{A_{sub_A}}, \tag{A.2}$$

where $n_{sub_A} = 1452$ is the number of atoms of the substrate, and $A_{sub_A} = 3.66$ nm $\times$ 3.66 nm is the substrate area. The averaged pressure at the substrate is found to be 100.69bar and 1000.004bar which validates the proposed pressure control algorithm.

Appendix B. Effects of controlling the pressure

As discussed above, besides the superheat temperature, surface topology and surface wettability, we believe that an imposed constant pressure is of great importance and will, at least, quantitatively affect the results of the simulation.

To support our claim, we re-examine the case with a hydrophilic nano-structured wall connected to a thermostat at 700K. The simulation setup is the same as the setup of the system in the manuscript but the piston is removed to avoid any control over the pressure.

Fig. B.12 displays the bubble nucleation, bubble growth, and the formation of the insulating film over the nano-structured hydrophilic wall with (first row) and without (second row) controlling the pressure.

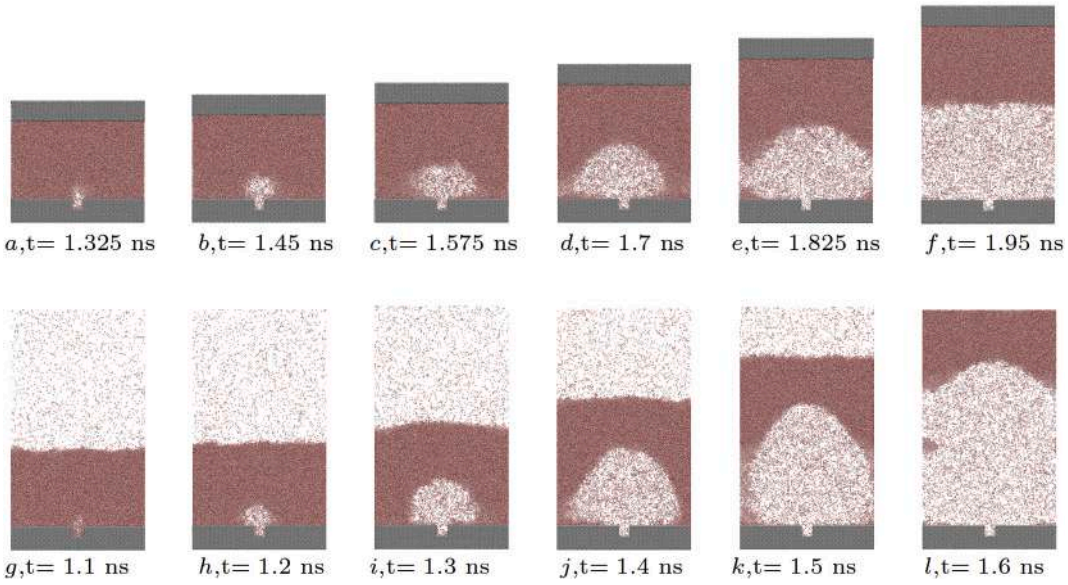

Fig. B.12. Evolution of the nucleated bubble over a hydrophilic nano-structured wall with (first row) and without (second row) controlling the pressure of the system. The thermostat temperature is set to $T_W = 700$ K. Controlling the pressure of the system affects the bubble nucleation, growth, and the film formation.

According to Fig. B.12, controlling the pressure of the system affects the results of the simulation. First, comparing Fig. B.12a and Fig. B.12g, the bubble nucleates sooner in the absence of the pressure control. This is consistent with the fundamental thermodynamical intuition: a bubble nucleates later at higher pressure. Second, without controlling the pressure, the bubble spreads faster and the insulating film of vapour forms sooner. The insulated film forms after 0.625 ns for the system under an imposed pressure (1*bar*), however, as at is illustrated in Fig. B.12g–Fig. B.12l, it takes about 0.5 ns for the nucleated bubble to grow and form the film if there is no control over the pressure. Finally, comparing B.12f and B.12l, we see that the film is much thicker in the absence of the pressure control algorithm.

Fig. B.13 shows the evolution of the averaged water temperature for the two systems. The filled circles indicate the nucleation instants. Without controlling the pressure of the system, the averaged temperature of the water slab is greater. This observations suggests that the pressure of the system also affects the rate of energy transfer to the system.

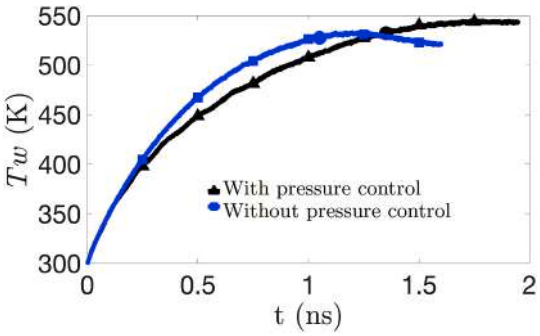

Fig. B.13. Effects of the system pressure on the evolution of the averaged temperature of the water slab. The filled circles correspond to the nucleation instant.

Based on the these results, we believe that a reliable pressure control mechanism is crucial when studying boiling heat transfer at nano-scales and our algorithm will therefore be useful also for future studies.

References

[1] J. Kim, Review of nucleate pool boiling bubble heat transfer mechanisms, Int. J. Multiphas. Flow 35 (12) (2009) 1067–1076, https://doi.org/10.1016/j.ijmultiphaseflow.2009.07.008. URL http://www.sciencedirect.com/science/article/pii/S0301932209001311.

[2] B. Agostini, M. Fabbri, J.E. Park, L. Wojtan, J.R. Thome, B. Michel, State of the art of high heat flux cooling technologies, arXiv: Heat Tran. Eng. 28 (4) (2007) 258–281, https://doi.org/10.1080/01457630601117799.

[3] J.R. Thome, Boiling in microchannels: a review of experiment and theory, Int. J. Heat Fluid Flow 25 (2) (2004) 128–139, selected Papers from the 5th ECI International Conference on Boiling Heat Transfer. doi:https://doi.org/10.1016/j.ijheatfluidflow.2003.11.005. URL http://www.sciencedirect.com/science/article/pii/S0142727X03001371.

[4] S. Gong, P. Cheng, Lattice Boltzmann simulation of periodic bubble nucleation, growth and departure from a heated surface in pool boiling, Int. J. Heat Mass Tran. 64 (2013) 122–132, https://doi.org/10.1016/j.ijheatmasstransfer.2013.03.058, http://www.sciencedirect.com/science/article/pii/S0017931013002652.

[5] S. Gong, P. Cheng, Numerical simulation of pool boiling heat transfer on smooth surfaces with mixed wettability by lattice Boltzmann method, Int. J. Heat Mass Tran. 80 (2015) 206–216, https://doi.org/10.1016/j.ijheatmasstransfer.2014.08.092. http://www.sciencedirect.com/science/article/pii/S001793101400790X.

[6] F. Magaletti, L. Marino, C.M. Casciola, Shock wave formation in the collapse of a vapor nanobubble, Phys. Rev. Lett. 114 (6) (2015), 064501.

[7] F. Magaletti, M. Gallo, L. Marino, C.M. Casciola, Shock-induced collapse of a vapor nanobubble near solid boundaries, Int. J. Multiphas. Flow 84 (2016) 34–45.

[8] B. Shen, J. Liu, G. Amberg, M. Do-Quang, J. Shiomi, K. Takahashi, Y. Takata, Contact-line behavior in boiling on a heterogeneous surface: physical insights from diffuse-interface modeling, Phys. Rev. Fluids 5 (2020), 033603, https://doi.org/10.1103/PhysRevFluids.5.033603. URL https://link.aps.org/doi/10.1103/PhysRevFluids.5.033603.

[9] C. Li, Z. Wang, P.-I. Wang, Y. Peles, N. Koratkar, G.P. Peterson, Nanostructured copper interfaces for enhanced boiling, Small 4 (8) (2008) 1084–1088, arXiv:

https://onlinelibrary.wiley.com/doi/pdf/10.1002/smll.200700991, doi:10.1002/smll.200700991, https://onlinelibrary.wiley.com/doi/abs/10.1002/smll.200700991.

[10] M. Zupančič, M. Može, P. Gregorčič, A. Sitar, I. Golobič, Evaluation of enhanced nucleate boiling performance through wall-temperature distributions on pdms-silica coated and non-coated laser textured stainless steel surfaces, Int. J. Heat Mass Tran. 111 (2017) 419–428, https://doi.org/10.1016/j.ijheatmasstransfer.2017.03.128. URL http://www.sciencedirect.com/science/article/pii/S0017931017306488.

[11] Y. Mao, Y. Zhang, Molecular dynamics simulation on rapid boiling of water on a hot copper plate, Appl. Therm. Eng. 62 (2) (2014) 607–612, doi:https://doi.org/10.1016/j.applthermaleng.2013.10.032. URL, http://www.sciencedirect.com/science/article/pii/S1359431113007412.

[12] K.F. Rabbi, S.I. Tamim, A.H.M. Faisal, K.M. Mukut, M.N. Hasan, A molecular dynamics study on thin film liquid boiling characteristics under rapid linear boundary heating: effect of liquid film thickness, AIP Conf. Proc. 1851 (1) (2017), 020102 arXiv:https://aip.scitation.org/doi/pdf/10.1063/1.4984731, doi:10.1063/1.4984731. URL, https://aip.scitation.org/doi/abs/10.1063/1.4984731.

[13] Y.-H. Wang, S.-Y. Wang, G. Lu, X.-D. Wang, Explosive boiling of nano-liquid argon films on high temperature platinum walls: effects of surface wettability and film thickness, Int. J. Therm. Sci. 132 (2018) 610–617, https://doi.org/10.1016/j.ijthermalsci.2018.07.007.

[14] Y.-H. Wang, S.-Y. Wang, G. Lu, X.-D. Wang, Effects of wettability on explosive boiling of nanoscale liquid films: whether the classical nucleation theory fails or not? Int. J. Heat Mass Tran. 132 (2019) 1277–1283, https://doi.org/10.1016/j.ijheatmasstransfer.2018.12.091.

[15] M. Gupta, A. Zou, S.C. Maroo, Onset and critical radius of heterogeneous bubble nucleation, Appl. Phys. Lett. 116 (10) (2020) 103704, https://doi.org/10.1063/1.5139961, arXiv:https://doi.org/10.1063/1.5139961, doi:10.1063/1.5139961. URL.

[16] A. Hens, R. Agarwal, G. Biswas, Nanoscale study of boiling and evaporation in a liquid ar film on a pt heater using molecular dynamics simulation, Int. J. Heat Mass Tran. 71 (2014) 303–312, doi:https://doi.org/10.1016/j.ijheatmasstransfer.2013.12.032. URL, http://www.sciencedirect.com/science/article/pii/S0017931013010764.

[17] W. Zhou, Y. Li, M. Li, J. Wei, W. Tao, Bubble nucleation over patterned surfaces with different wettabilities: molecular dynamics investigation, Int. J. Heat Mass Tran. 136 (2019) 1–9, https://doi.org/10.1016/j.ijheatmasstransfer.2019.02.093. URL http://www.sciencedirect.com/science/article/pii/S0017931018350257.

[18] N. Wu, L. Zeng, T. Fu, Z. Wang, C. Lu, Molecular dynamics study of rapid boiling of thin liquid water film on smooth copper surface under different wettability conditions, Int. J. Heat Mass Tran. 147 (2020) 118905, doi:https://doi.org/10.1016/j.ijheatmasstransfer.2019.118905. URL, http://www.sciencedirect.com/science/article/pii/S0017931019324251.

[19] T. Fu, Y. Mao, Y. Tang, Y. Zhang, W. Yuan, Molecular dynamics simulation on rapid boiling of thin water films on cone-shaped nanostructure surfaces, Nanoscale Microscale Thermophys. Eng. 19 (1) (2015) 17–30, https://doi.org/10.1080/15567265.2014.991480, arXiv:https://doi.org/10.1080/15567265.2014.991480, doi:10.1080/15567265.2014.991480. URL.

[20] S. Mukherjee, S. Datta, A. Kumar Das, Molecular dynamic study of boiling heat transfer over structured surfaces, J. Heat Tran. 140 (5) (02 2018), 054503, https://doi.org/10.1115/1.4038480 arXiv:https://asmedigitalcollection.asme.org/heattransfer/article-pdf/140/5/054503/6217944/ht_140_05_054503.pdf, doi:10.1115/1.4038480.

[21] L. Zhang, J. Xu, G. Liu, J. Lei, Nucleate boiling on nanostructured surfaces using molecular dynamics simulations, Int. J. Therm. Sci. 152 (2020) 106325, doi:https://doi.org/10.1016/j.ijthermalsci.2020.106325. URL http://www.sciencedirect.com/science/article/pii/S1290072918321550.

[22] S. Zhang, F. Hao, H. Chen, W. Yuan, Y. Tang, X. Chen, Molecular dynamics simulation on explosive boiling of liquid argon film on copper nanochannels, Appl. Therm. Eng. 113 (2017) 208–214, https://doi.org/10.1016/j.applthermaleng.2016.11.034. URL, http://www.sciencedirect.com/science/article/pii/S135943111633068X.

[23] Y. Chen, J. Li, B. Yu, D. Sun, Y. Zou, D. Han, Nanoscale study of bubble nucleation on a cavity substrate using molecular dynamics simulation, Langmuir 34 (47) (2018) 14234–14248, https://doi.org/10.1021/acs.langmuir.8b03044, pMID: 30398360. arXiv:https://doi.org/10.1021/acs.langmuir.8b03044, doi:10.1021/acs.langmuir.8b03044. URL.

[24] R. Diaz, Z. Guo, Molecular dynamics study of wettability and pitch effects on maximum critical heat flux in evaporation and pool boiling heat transfer, Numer. Heat Tran., Part A: Applications 72 (12) (2017) 891–903, https://doi.org/10.1080/10407782.2017.1412710, arXiv:https://doi.org/10.1080/10407782.2017.1412710, doi:10.1080/10407782.2017.1412710. URL.

[25] Y.-J. Chen, B. Yu, Y. Zou, B.-N. Chen, W.-Q. Tao, Molecular dynamics studies of bubble nucleation on a grooved substrate, Int. J. Heat Mass Tran. 158 (2020) 119850, https://doi.org/10.1016/j.ijheatmasstransfer.2020.119850.

[26] S. Marchio, S. Meloni, A. Giacomello, C. Valeriani, C.M. Casciola, Pressure control in interfacial systems: atomistic simulations of vapor nucleation, J. Chem. Phys. 148 (6) (2018), 064706, https://doi.org/10.1063/1.5011106 arXiv:https://doi.org/10.1063/1.5011106, doi:10.1063/1.5011106. URL.

[27] B.L. Holian, A.F. Voter, R. Ravelo, Thermostatted molecular dynamics: how to avoid the toda demon hidden in nosé-hoover dynamics, Phys. Rev. E 52 (1995) 2338–2347, https://doi.org/10.1103/PhysRevE.52.2338. URL https://link.aps.org/doi/10.1103/PhysRevE.52.2338.

[28] H.J.C. Berendsen, J.R Grigera, T.P Straatsma, The missing term in effective pair potentials, J. Phys. Chem. 91 (1987) 6269–6271.

[29] G. Nagayama, M. Kawagoe, A. Tokunaga, T. Tsuruta, On the evaporation rate of ultra-thin liquid film at the nanostructured surface: a molecular dynamics study, Int. J. Therm. Sci. 49 (1) (2010) 59–66, https://doi.org/10.1016/j.ijthermalsci.2009.06.001. URL http://www.sciencedirect.com/science/article/pii/S1290072909001409.

[30] J.H. Weijs, A. Marchand, B. Andreotti, D. Lohse, J.H. Snoeijer, Origin of line tension for a Lennard-Jones nanodroplet, Phys. Fluids 23 (2) (2011), 022001, https://doi.org/10.1063/1.3546008 arXiv:https://doi.org/10.1063/1.3546008, doi:10.1063/1.3546008. URL.

[31] M.J. Abraham, T. Murtola, R. Schulz, S. Páll, J.C. Smith, B. Hess, E. Lindahl, Gromacs: high performance molecular simulations through multi-level parallelism from laptops to supercomputers, SoftwareX 1–2 (2015) 19–25, https://doi.org/10.1016/j.softx.2015.06.001. URL http://www.sciencedirect.com/science/article/pii/S2352711015000059.

[32] M. Parrinello, A. Rahman, Polymorphic transitions in single crystals: a new molecular dynamics method, J. Appl. Phys. 52 (12) (1981) 7182–7190, https://doi.org/10.1063/1.328693, arXiv:https://doi.org/10.1063/1.328693, doi:10.1063/1.328693. URL.

[33] A. Cassie, S. Baxter, Wettability of porous surfaces, Trans. Faraday Soc. 40 (1944) 546–551.

[34] R.N. Wenzel, Resistance of solid surfaces to wetting by water, Ind. Eng. Chem. 28 (1936) 988–994.

[35] A. Giacomello, M. Chinappi, S. Meloni, C.M. Casciola, Metastable wetting on superhydrophobic surfaces: continuum and atomistic views of the cassie-baxter–wenzel transition, Phys. Rev. Lett. 109 (2012) 226102, https://doi.org/10.1103/PhysRevLett.109.226102. URL https://link.aps.org/doi/10.1103/PhysRevLett.109.226102.

[36] S. Meloni, A. Giacomello, C.M. Casciola, Focus article: theoretical aspects of vapor/gas nucleation at structured surfaces, J. Chem. Phys. 145 (21) (2016) 211802.

[37] S. Das, B. Saha, S. Bhaumik, Experimental study of nucleate pool boiling heat transfer of water by surface functionalization with sio2 nanostructure, Exp. Therm. Fluid Sci. 81 (2017) 454–465, https://doi.org/10.1016/j.expthermflusci.2016.09.009. URL http://www.sciencedirect.com/science/article/pii/S0894177716302552.